THREE-TIME-LEVEL SEMI-LAGRANGIAN SCHEMES IN FINITE-ELEMENT AND SPECTRAL MODELS

Clive Temperton and Harold Ritchie
Division de Recherche en Prévision Numérique
Service de l'Environnement Atmosphérique
Dorval, Québec, Canada H9P 1J3

1. INTRODUCTION

A long-standing problem in the integration of numerical weather prediction models, using the primitive equations, is that the maximum permissible timestep has always been governed by considerations of stability rather than accuracy; for the integration to be stable, the timestep has to be so small that the time-truncation error is very much smaller than the spatial truncation error.

The situation improved considerably following the development of semi-implicit time integration schemes (Robert, 1969; Kwizak and Robert, 1971; Robert et al., 1972). By treating the linear terms responsible for high-frequency oscillations in an implicit manner, it was possible to use timesteps six times longer than for the earlier explicit leapfrog schemes, with no loss of accuracy. Nevertheless, the maximum stable timestep remained much smaller than seemed necessary from considerations of accuracy alone.

Robert (1981, 1982) proposed combining the semi-implicit integration scheme with a semi-Lagrangian treatment of the advection terms in a barotropic model, and more recently Robert et al. (1985) extended this scheme to a multi-level model. They found that the timestep could be increased by a further factor of six over that for an Eulerian semi-implicit scheme, in

the context of a finite-difference model defined on a horizontally uniform grid.

In this paper we adapt Robert's technique, both to a regional finite-element model with variable resolution and to a global spectral model. Following Robert, these applications are based on combining the semi-Lagrangian treatment of advection with a three-time-level semi-implicit scheme. It is also possible to construct two-time-level semi-Lagrangian semi-implicit schemes; these are presented in a companion paper by Staniforth and Côté (1988).

2. A SEMI-IMPLICIT SEMI-LAGRANGIAN SCHEME

In order to prepare the ground for later developments, we first illustrate the application of a semi-implicit semi-Lagrangian scheme to the shallow-water equations on a polar stereographic projection, without explicitly considering the details of the horizontal discretization.

Let x and y be the coordinates of the projection; u and v are the x- and y-components of the wind vector, ϕ is the perturbation geopotential, Φ_0 is the mean geopotential, m is the map scale factor and f is the Coriolis parameter. Defining wind images U = u/m, V = v/m, the equations take the form:

$$\frac{dU}{dt} - fV + \frac{\partial \phi}{\partial x} + K\frac{\partial S}{\partial x} = 0 \qquad (2.1)$$

$$\frac{dV}{dt} + fU + \frac{\partial \phi}{\partial y} + K\frac{\partial S}{\partial y} = 0 \qquad (2.2)$$

$$\frac{d\phi}{dt} + \Phi_0 D + \phi D = 0 \qquad (2.3)$$

where $K = \tfrac{1}{2}(U^2 + V^2)$, $S = m^2$, $D = S\left(\frac{\partial U}{\partial x} + \frac{\partial V}{\partial y}\right)$ and

$$\frac{d}{dt} \equiv \frac{\partial}{\partial t} + S\left(U\frac{\partial}{\partial x} + V\frac{\partial}{\partial y}\right).$$

Suppose now that the model variables U, V, ϕ are defined at a set of grid points at time-levels t and $(t-\Delta t)$, and that the integration is to be carried forward to time-level $(t+\Delta t)$. For each gridpoint $\underset{\sim}{x}$, we consider the trajectory of a particle which arrives at $\underset{\sim}{x}$ at time $(t+\Delta t)$, and we

approximate this trajectory by a straight line in (x,y) space over the time interval $[t-\Delta t,\ t+\Delta t]$, as illustrated in Fig. 1. Thus in (x, y, t) space, the trajectory begins at $(\underset{\sim}{x}-2\underset{\sim}{\alpha},\ t-\Delta t)$ and ends at $(\underset{\sim}{x},\ t+\Delta t)$.

To implement the semi-Lagrangian algorithm, the first step is to find $\underset{\sim}{\alpha}$ for each gridpoint $\underset{\sim}{x}$. A time- and space-centred discretization of $\underset{\sim}{v} = d\underset{\sim}{x}/dt$ along the trajectory yields the equation defining $\underset{\sim}{\alpha}$:

$$\underset{\sim}{v}(\underset{\sim}{x} - \underset{\sim}{\alpha},\ t) = \frac{2\underset{\sim}{\alpha}}{2\Delta t},$$

i.e.

$$\underset{\sim}{\alpha} = \Delta t\,\underset{\sim}{v}(\underset{\sim}{x}-\underset{\sim}{\alpha},\ t). \tag{2.4}$$

Since Eq. (2.4) is implicit, Robert (1981) suggested the following simple iterative scheme:

$$\underset{\sim}{\alpha}^{(k+1)} = \Delta t \cdot \underset{\sim}{v}(\underset{\sim}{x}-\underset{\sim}{\alpha}^{(k)},\ t) \tag{2.5}$$

where k is the iteration number. If $\underset{\sim}{\alpha}^{(o)}$ is taken to be the value found at the previous timestep, then two iterations are usually found to be sufficient. Since $\underset{\sim}{x}-\underset{\sim}{\alpha}$ is not in general a gridpoint, the right-hand side of (2.5) has to be evaluated by a suitable interpolation scheme; for this stage of the computation, bilinear interpolation seems to be adequate.

Once $\underset{\sim}{\alpha}$ has been found, the total derivative in (2.1) can be approximated by

$$\frac{dU}{dt} \rightarrow \frac{U^+ - U^-}{2\Delta t}$$

where

$$U^+ = U(\underset{\sim}{x},\ t+\Delta t) \tag{2.6}$$

$$U^- = U(\underset{\sim}{x}-2\underset{\sim}{\alpha},\ t-\Delta t) \tag{2.7}$$

and similarly for dV/dt in (2.2) and $d\phi/dt$ in (2.3). The values U^-, V^-, ϕ^- again must be found by interpolation of the fields at $(t-\Delta t)$; this time a more accurate interpolation scheme (e.g., bicubic) is necessary to avoid smoothing the fields.

The semi-implicit part of the scheme consists of averaging the pressure-gradient terms in (2.1) and (2.2), and the $\Phi_0 D$ term in (2.3),

along the trajectory; thus for example in (2.1),

$$\frac{\partial \phi}{\partial x} \rightarrow \frac{1}{2}\left[\left(\frac{\partial \phi}{\partial x}\right)^{+} + \left(\frac{\partial \phi}{\partial x}\right)^{-}\right].$$

The remaining terms in the equations will be evaluated at time-level t and half-way along the trajectory, at $\underset{\sim}{x}-\underset{\sim}{\alpha}$; to (2.6) and (2.7) we add the notation

$$U^{\circ} = U(\underset{\sim}{x}-\underset{\sim}{\alpha},\ t). \tag{2.8}$$

Eqs. (2.1)-(2.3) are thus discretized as follows:

$$\frac{U^{+} - U^{-}}{2\Delta t} - fV^{\circ} + \frac{1}{2}\left[\left(\frac{\partial \phi}{\partial x}\right)^{+} + \left(\frac{\partial \phi}{\partial x}\right)^{-}\right] + \left(K\frac{\partial S}{\partial x}\right)^{\circ} = 0 \tag{2.9}$$

$$\frac{V^{+} - V^{-}}{2\Delta t} + fU^{\circ} + \frac{1}{2}\left[\left(\frac{\partial \phi}{\partial y}\right)^{+} + \left(\frac{\partial \phi}{\partial y}\right)^{-}\right] + \left(K\frac{\partial S}{\partial y}\right)^{\circ} = 0 \tag{2.10}$$

$$\frac{\phi^{+} - \phi^{-}}{2\Delta t} + \tfrac{1}{2}\,\Phi_0\left[D^{+} + D^{-}\right] + (\phi D)^{\circ} = 0. \tag{2.11}$$

Notice that the system (2.9)-(2.11) is completely centred in time and space, thus maintaining the second-order accuracy in time of the Eulerian semi-implicit scheme.

Once $\underset{\sim}{\alpha}$ has been found for each gridpoint, all the terms in (2.9)-(2.11) defined at $(\underset{\sim}{x}-\underset{\sim}{\alpha},\ t)$ and $(\underset{\sim}{x}-2\underset{\sim}{\alpha},\ t-\Delta t)$ can be evaluated. Putting all these "known" terms on the right-hand side, Eqs. (2.9)-(2.11) take the form:

$$\left(U + \Delta t\frac{\partial \phi}{\partial x}\right)^{+} = R_1 \tag{2.12}$$

$$\left(V + \Delta t\frac{\partial \phi}{\partial y}\right)^{+} = R_2 \tag{2.13}$$

$$\left(\phi + \Phi_0 \Delta t D\right)^{+} = R_3 \tag{2.14}$$

To solve this system, we take $\frac{\partial}{\partial x}$ (2.12) + $\frac{\partial}{\partial y}$ (2.13) and substitute for D^{+} in (2.15), yielding a Helmholtz equation for ϕ^{+}:

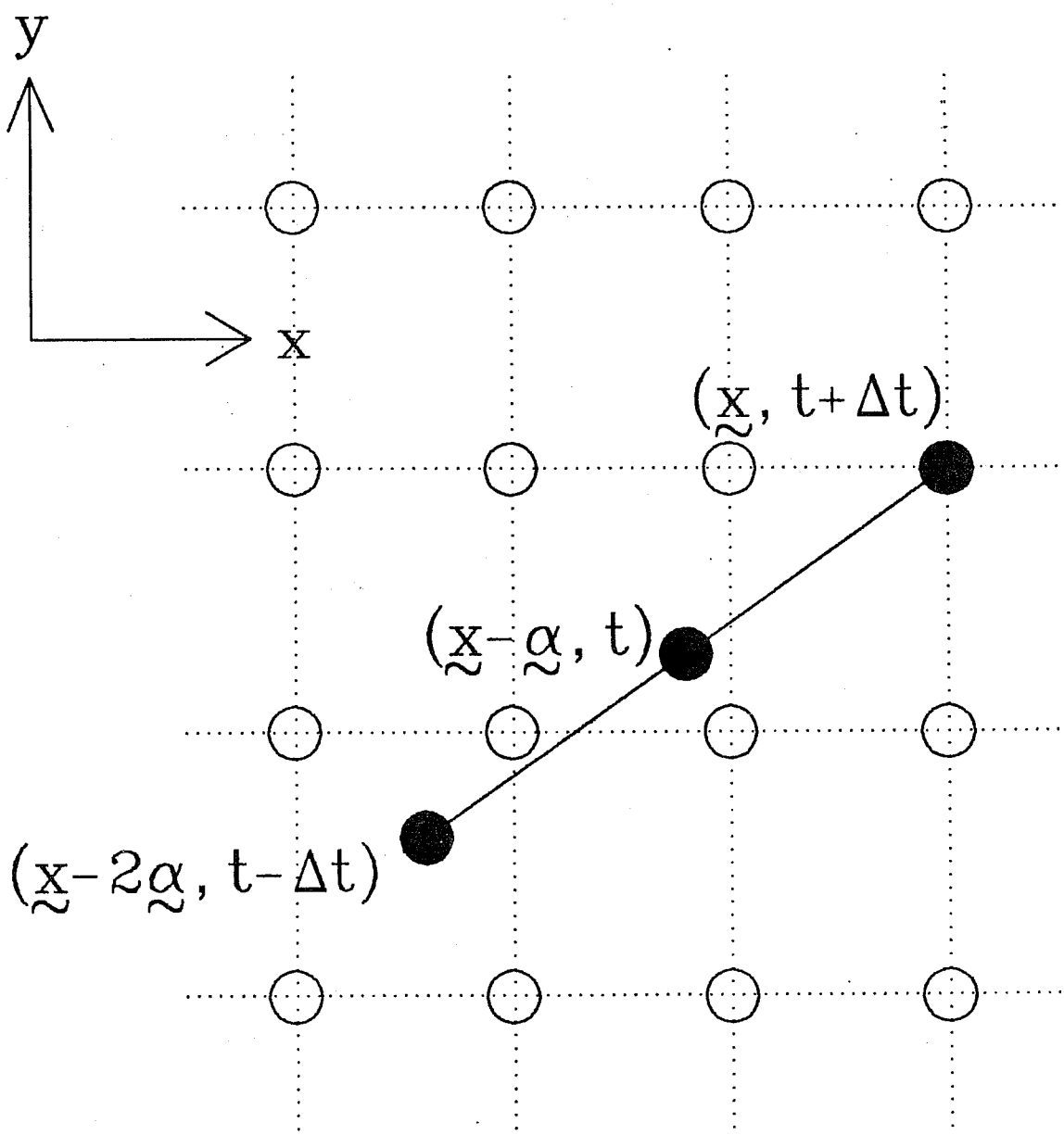

Fig. 1 The approximated trajectory as used in a three-time-level semi-Lagrangian scheme.

$$\left[\frac{\partial^2}{\partial x^2} + \frac{\partial^2}{\partial y^2} - \frac{1}{\Phi_0 S(\Delta t)^2}\right] \phi^+ = R_4. \qquad (2.15)$$

Once (2.15) has been solved for ϕ^+, the new wind image fields U^+ and V^+ can in principle be found by substituting back in (2.12) and (2.13), and the timestep is completed.

A "non-interpolating" variant of the scheme has also been proposed (Ritchie, 1986). In this approach, we first find $\underset{\sim}{\alpha}$ using (2.5) (which does require interpolation) and then define $\underset{\sim}{\alpha}^*$ such that $\underset{\sim}{x}-2\underset{\sim}{\alpha}^*$ is the nearest grid point to $\underset{\sim}{x}-2\underset{\sim}{\alpha}$. The advecting wind is then split into two parts:

$$\underset{\sim}{v} = \underset{\sim}{v}^* + \underset{\sim}{v}'$$

where $\underset{\sim}{v}^* = \underset{\sim}{\alpha}^*/\Delta t$, and terms such as $d\phi/dt$ are approximated by

$$\frac{d\phi}{dt} \rightarrow \frac{\phi^+-\phi^-}{2\Delta t} + \left[S\left(U'\frac{\partial \phi}{\partial x} + V'\frac{\partial \phi}{\partial y}\right)\right]^0 \qquad (2.16)$$

with the notations of (2.7) and (2.8) now replaced by

$$U^- = U\left(\underset{\sim}{x}-2\underset{\sim}{\alpha}^*,\ t-\Delta t\right), \qquad (2.17)$$

$$U^0 = U\left(\underset{\sim}{x}-\underset{\sim}{\alpha}^*,\ t\right) \qquad (2.18)$$

and $(U')^0$ in (2.16) defined by

$$(U')^0 = U^0 - U^*.$$

The remaining terms in the equations are again evaluated as in (2.9)-(2.11), but using the new definitions (2.17) and (2.18) for the quantities evaluated at time-levels t and $(t-\Delta t)$. Again a system of the form (2.12)-(2.14) is obtained, and the timestep is completed in the same way.

This non-interpolating version has two potential advantages. First, the quantities at $(t-\Delta t)$ are defined at gridpoints, so no interpolation is required to evaluate them, and the smoothing effects (and the cost) of interpolation are eliminated. Second, on a uniform grid the quantities at time t, as in Eq. (2.18), are defined either at gridpoints or halfway

between them, so they can be evaluated by simple interpolation formulae.

The viability of the "non-interpolating" semi-Lagrangian scheme was demonstrated by Ritchie (1986) both for a passive advection problem and in a semi-implicit shallow-water equation model.

3. APPLICATION TO A FINITE-ELEMENT MODEL

Since Robert (1981, 1982), Robert et al. (1985), and Ritchie (1986) had so clearly demonstrated the advantages of a semi-Lagrangian semi-implicit scheme in a gridpoint model, it was natural to ask whether it could be extended to models using other forms of horizontal discretization. The first such application was described by Staniforth and Temperton (1986).

The model in this case was the regional barotropic finite-element model of Staniforth and Mitchell (1977, 1978). The domain of the model is quasi-hemispheric, with a solid-wall boundary in the vicinity of the equator, and a variable-resolution grid with uniform high resolution over the region of interest (see Fig. 2). The discretization is based on bilinear finite elements.

In trying to apply a semi-Lagrangian semi-implicit scheme to this model, an immediate problem is that the Eulerian version of the model is based not on the momentum form of the equations as in (2.1)-(2.2) but on their differentiated (vorticity-divergence) form; the reasons for this choice are discussed in Staniforth and Mitchell (1977). The essence of the semi-Lagrangian scheme lies in the treatment of the advective terms; the vorticity equation has a natural advective form which is appropriate for semi-Lagrangian treatment, but the divergence equation does not contain suitable advection terms.

Two solutions to this problem, differing only in their treatment of the rotational part of the wind field, were proposed by Staniforth and Temperton (1986). The U, V and ϕ equations were first written in the form (2.9)-(2.11), or equivalently (2.12)-(2.14); all derivatives and products appearing in the right-hand sides R_1, R_2, R_3 were evaluated using the

bilinear finite-element basis. Adding the (discrete) x-derivative of (2.12) to the corresponding y-derivative of (2.13) gives

$$(D/S)^+ = -\Delta t(\phi_{xx} + \phi_{yy})^+ + (R_1)_x + (R_2)_y \qquad (3.1)$$

and substituting in (2.14) gives a discrete form of the Helmholtz equation (2.15):

$$\left[\phi_{xx} + \phi_{yy} - \frac{\phi}{\Phi_0 S(\Delta t)^2}\right]^+ = R_4. \qquad (3.2)$$

As shown by Staniforth and Temperton (1986), the boundary conditions for this Helmholtz equation are obtained by setting the normal component of the wind images at time $(t+\Delta t)$ to zero at the boundary.

After (3.2) has been solved for ϕ^+, the right-hand side of (3.1) can be evaluated explicitly, and the divergent component (U_d, V_d) of the wind field at $(t+\Delta t)$ can be found by solving a Poisson equation for the velocity potential χ^+:

$$(\chi_{xx} + \chi_{yy})^+ = (D/S)^+ \qquad (3.3)$$

with Neumann boundary conditions (zero normal derivatives). After solving (3.3), we set

$$(U_d)^+ = \chi_x^+ , \quad (V_d)^+ = \chi_y^+. \qquad (3.4)$$

As mentioned above, the two proposed schemes differed in their treatment of the rotational wind field. For Scheme A, the y-derivative of (2.12) was subtracted from the x-derivative of (2.13) to give

$$(\zeta/S)^+ = (\psi_{xx} + \psi_{yy})^+ = (R_2)_x - (R_1)_y \qquad (3.5)$$

where

$$\zeta = S\left(\frac{\partial V}{\partial x} - \frac{\partial U}{\partial y}\right).$$

Hence the Poisson equation (3.5) may be solved for ψ^+ (using Dirichlet boundary conditions), and the rotational component (U_r, V_r) of the wind field at $(t+\Delta t)$ found from

$$(U_r)^+ = -\psi_y^+ , \quad (V_r)^+ = \psi_x^+ , \qquad (3.6)$$

thus completing the timestep.

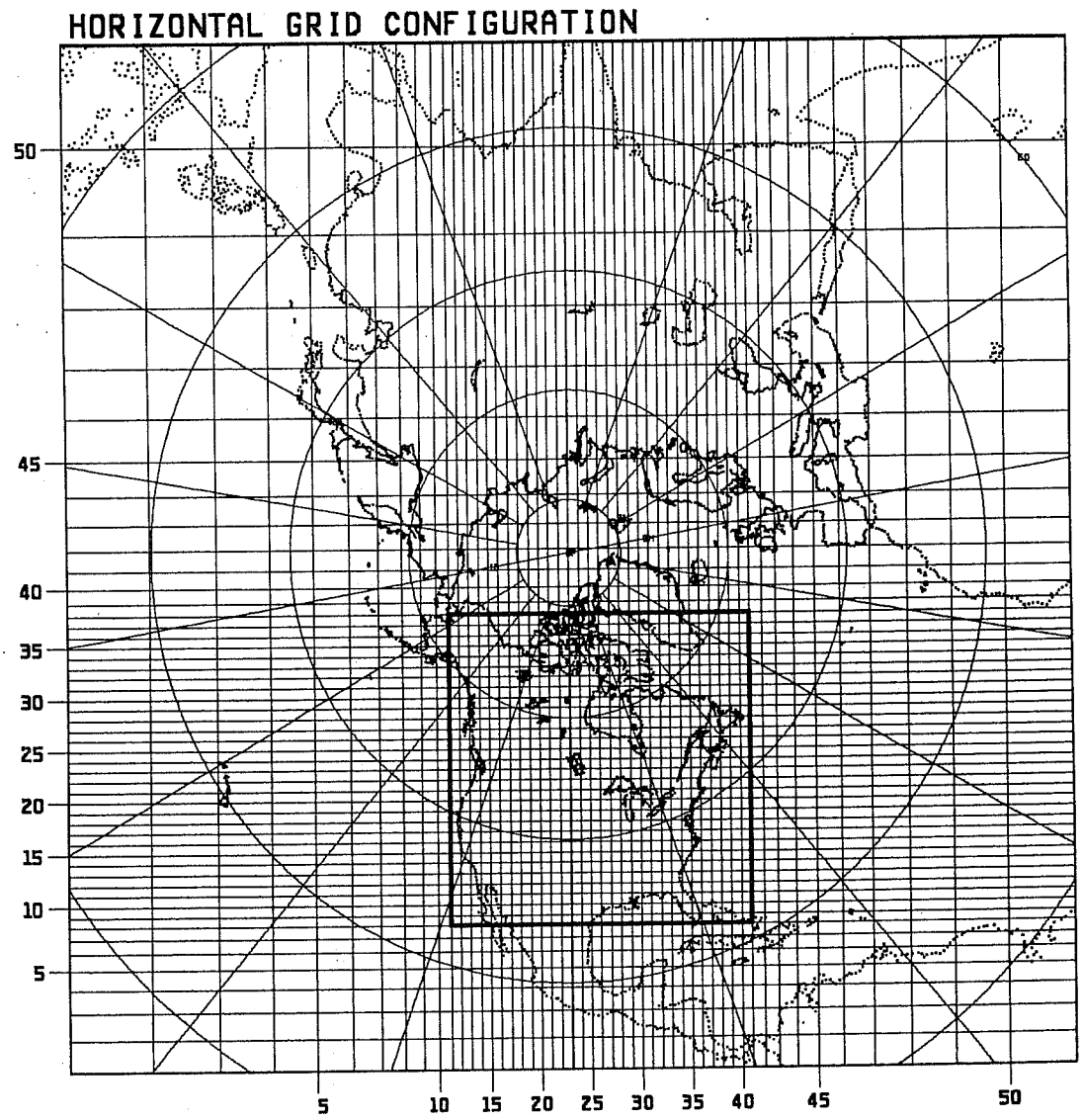

Fig. 2 The 101 x 101 non-uniform grid of the finite-element model. For clarity, only every other line of the mesh is shown.

(a)

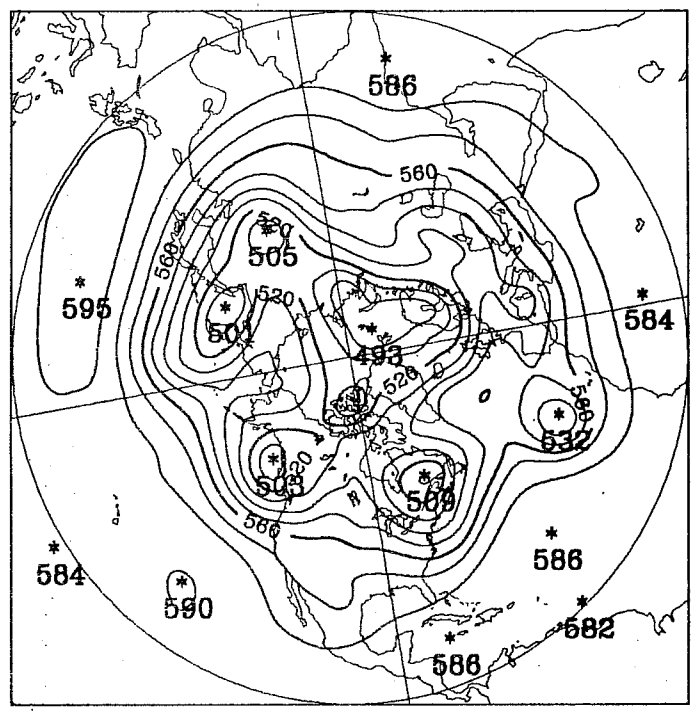

CONTROL RUN ON UNIFORM GRID DAY 2

(b)

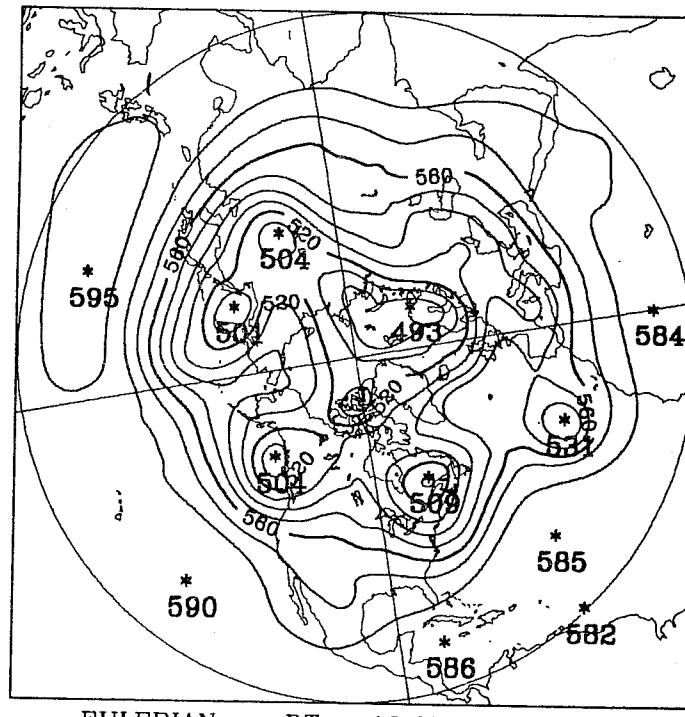

EULERIAN DT = 10 MIN DAY 2

Fig. 3 48-hour forecast height fields: (a) control run on uniform grid, (b) Eulerian run on non-uniform grid (Δt = 10 min). Contour interval 10 dam.

(c)

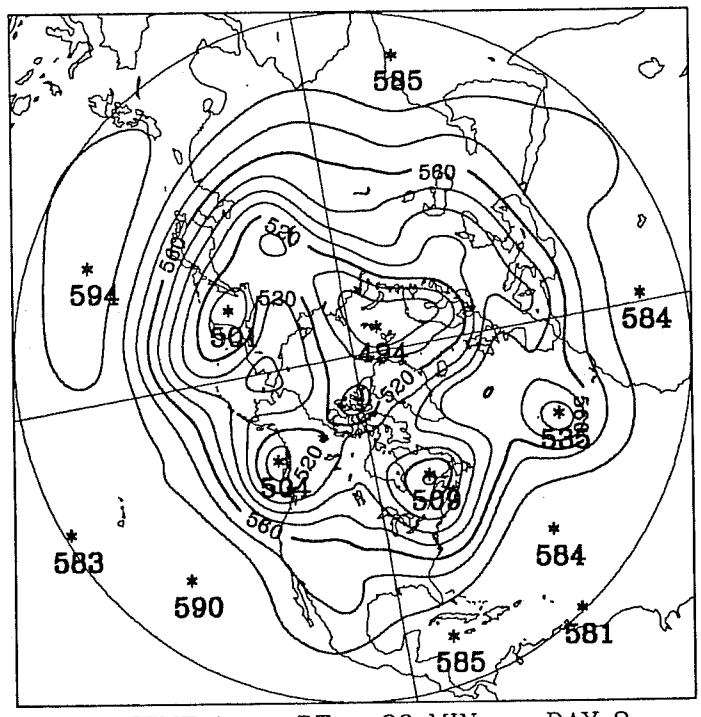

SCHEME A DT = 90 MIN DAY 2

(d)

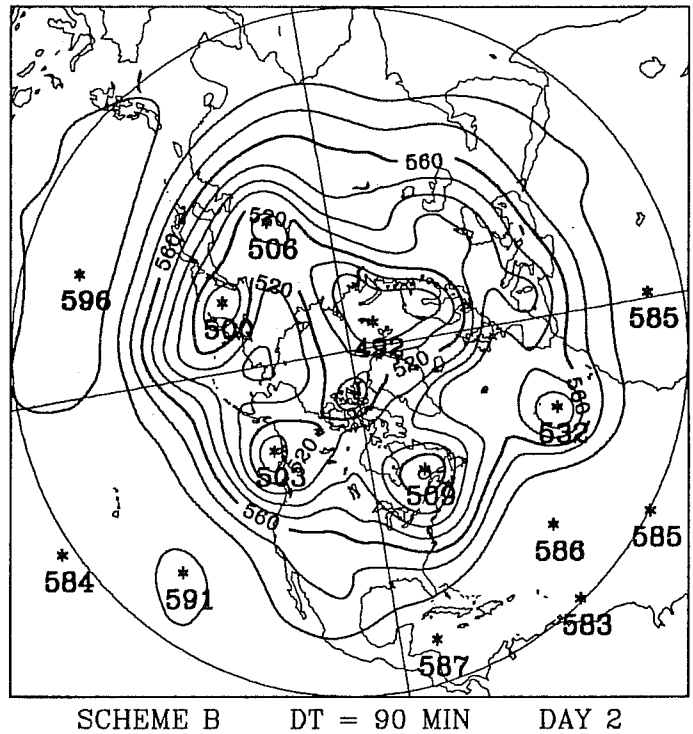

SCHEME B DT = 90 MIN DAY 2

Fig. 3 (continued). 48-hour forecast height fields: (c) Scheme A, (d) Scheme B, both with Δt = 90 min. Contour interval 10 dam.

For Scheme B, an alternative method was used to update the rotational part of the wind field. Taking the curl of Eqs. (2.1) and (2.2) gives a vorticity equation in advective form:

$$\frac{dQ}{dt} = -QD \tag{3.7}$$

where $Q = \zeta+f$. A semi-Lagrangian discretization of (3.7) gives

$$\frac{Q^+ - Q^-}{2\Delta t} = -(QD)^\circ,$$

from which we obtain

$$(\psi_{xx} + \psi_{yy})^+ = \left[Q^- - 2\Delta t(QD)^\circ - f^+\right]/S^+. \tag{3.8}$$

The solution procedure for Scheme B proceeds as in Scheme A, except that (3.8) rather than (3.5) is solved for ψ^+.

A linear stability analysis of the two schemes was presented by Staniforth and Temperton (1986). The principal conclusions were as follows: Scheme A is stable for $|f\Delta t| \leq 1$, but there is an $O(\Delta x^4)$ damping of the slow modes each timestep, independent of Δt. This results essentially from an inconsistency in the way the vorticity is derived from the stream function at time-levels $(t+\Delta t)$ and $(t-\Delta t)$; for the linear finite-element scheme, taking a first derivative twice gives a different result from taking a second derivative (the situation is analogous to that on an unstaggered finite-difference grid). For Scheme B, the linear analysis gives stability for $|f\Delta t| \leq 0.966$ (this value appears instead of 1 as a consequence of using a fourth-order accurate approximation of the Laplacian in (3.8)), and neutrally stable slow modes. On the basis of this analysis, the two schemes should have similar stability properties; but Scheme A is shown to yield damped solutions.

To compare the performance of the Eulerian and semi-Lagrangian forms of the barotropic finite-element model, Staniforth and Temperton (1986) carried out a series of experiments over a square domain of side 20 000 km, using a polar stereographic projection. A control integration was run on a uniform 201 x 201 (100 km) mesh, using the Eulerian formulation of Staniforth and Mitchell (1977, 1978) with a timestep of Δt = 10 minutes. The "experimental" integrations were run on a variable-resolution 101 x 101 grid, which coincided with the uniform mesh of the control experiment over

the region of interest. Since Robert et al. (1985) had identified the lack of a proper initialization procedure as a source of difficulty in measuring the time-truncation error of a semi-Lagrangian scheme, the initial fields (derived from a 500 mb analysis) were carefully balanced for both the control and experimental runs.

Experiments were first performed to examine the stability of the schemes on the non-uniform grid. For the Eulerian version of the model, the maximum stable timestep was found to be between 12 and 15 minutes. In complete contrast, both the semi-Lagrangian schemes A and B were found to be stable with timesteps of 90 minutes.

To examine the accuracy of the schemes a series of 48-hour integrations was run on the non-uniform grid, using the Eulerian scheme (Δt = 10 minutes) and the semi-Lagrangian schemes A and B (Δt = 10, 20, 30, 45, 60 and 90 minutes). These integrations were then compared with the uniform-grid control run. Fig. 3 shows the 48-hour forecast height field from the control run, the Eulerian scheme, and the two semi-Lagrangian schemes with Δt = 90 minutes. Clearly, the control forecast is quite accurately reproduced by all three runs on the non-uniform grid.

R.m.s. differences were computed between each forecast on the non-uniform grid and the control forecast on the high-resolution uniform grid, over the area of interest. These are presented in Fig. 4, as a function of timestep length. For a 10-minute timestep, the semi-Lagrangian Scheme B reproduces the control forecast more accurately than the Eulerian scheme, which is already close to its stability limit. Moreover, for Scheme B there is little or no deterioration in accuracy as the timestep is extended to at least 60 minutes, and the accuracy remains acceptable even with a timestep of 90 minutes. Scheme A behaves quite differently; with short timesteps the damping results in a serious loss of accuracy. As the timestep increases to 45-60 minutes the errors become less serious, but the accuracy never matches that of either the Eulerian model or the semi-Lagrangian Scheme B.

A further interesting demonstration of the accuracy of Scheme B is given in Fig. 5, which shows maps of the differences from the control run,

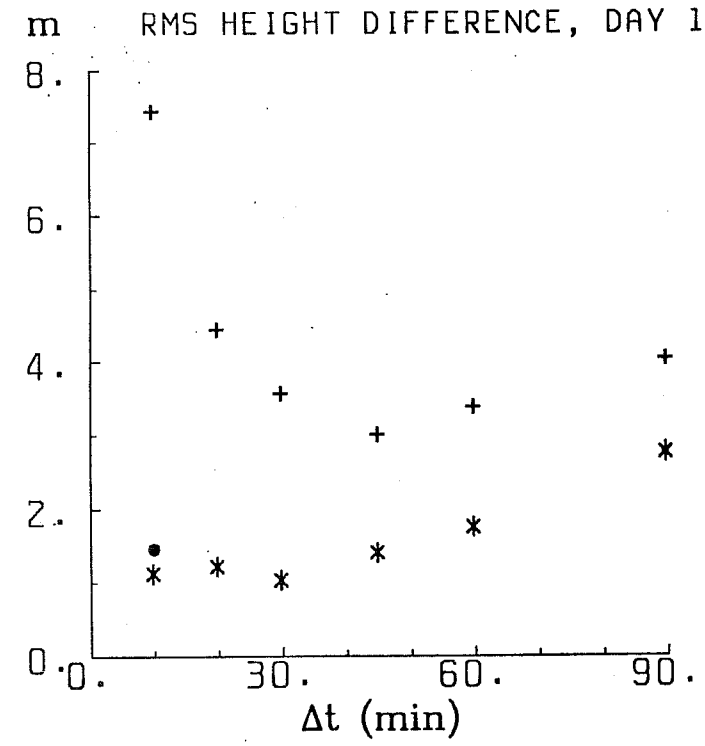

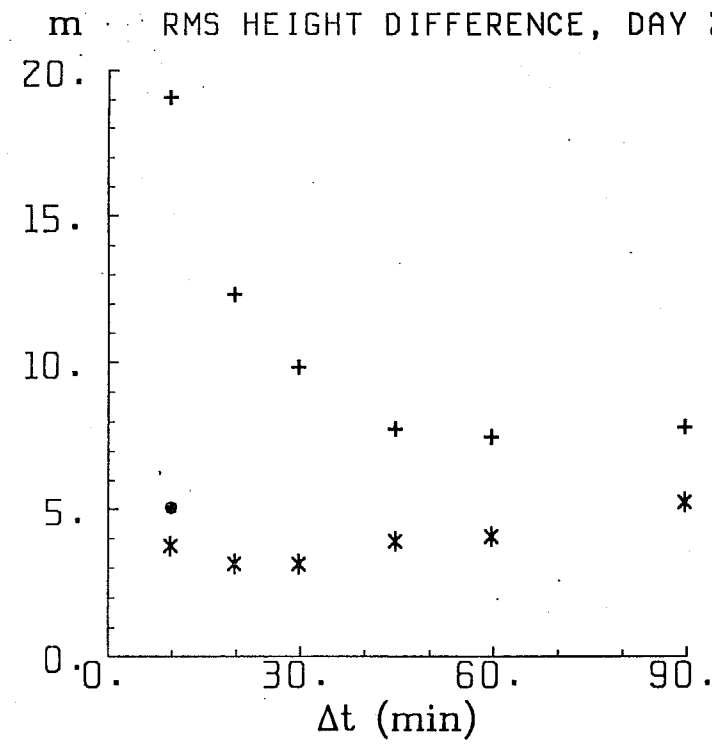

Fig. 4 Rms differences from the control run, over the region of interest, as a function of Δt: height fields.
• Eulerian, + Scheme A, * Scheme B.

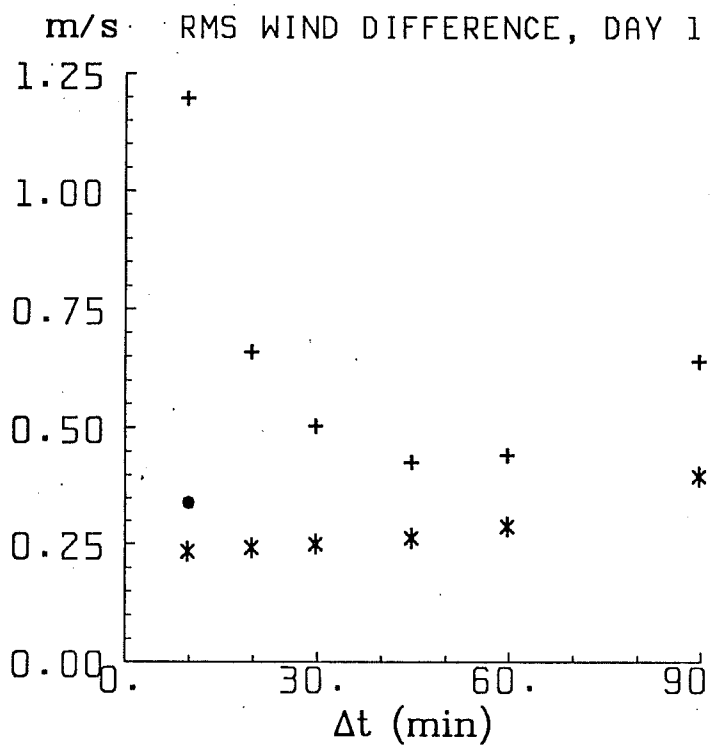

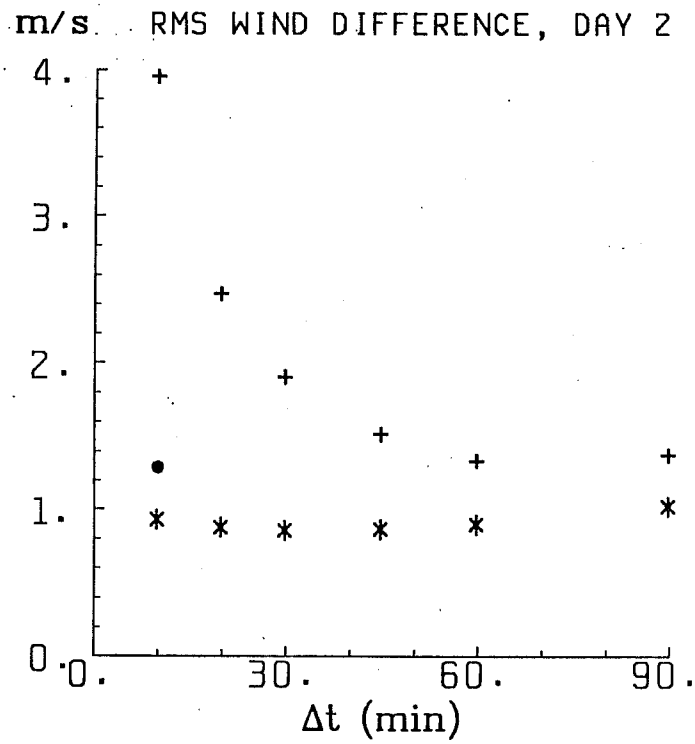

Fig. 4 (continued). Rms differences from the control run, over the region of interest, as a function of Δt: wind fields. • Eulerian, + Scheme A, * Scheme B.

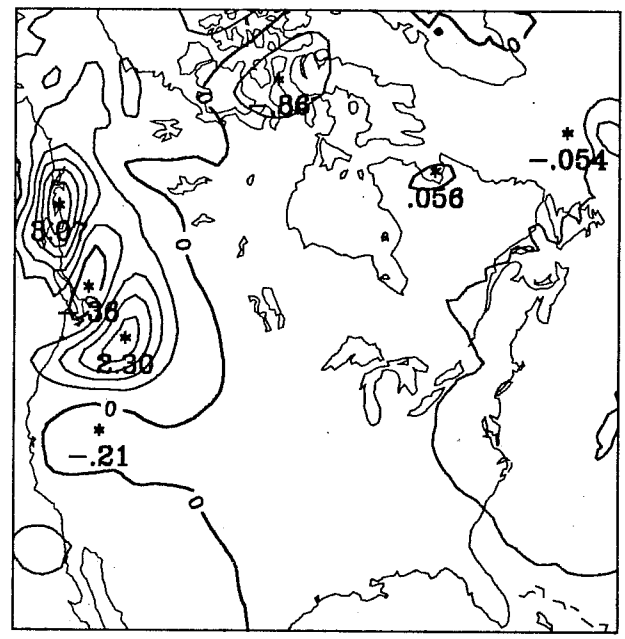

EULERIAN MINUS CONTROL DAY 2

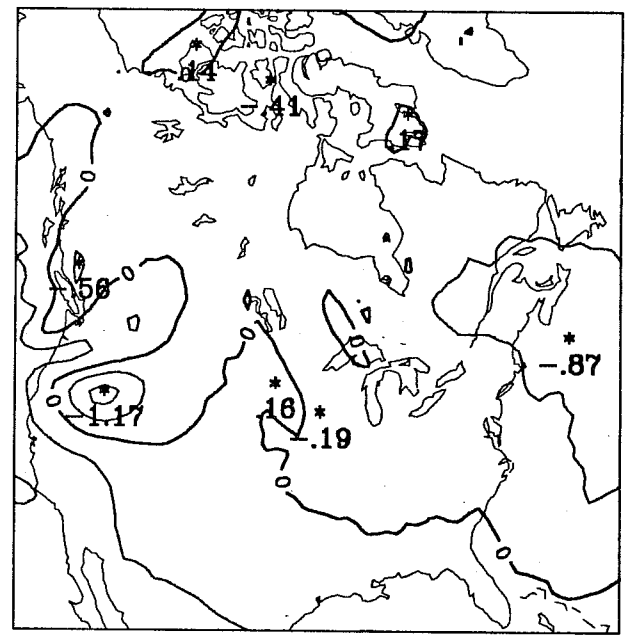

SCHEME B MINUS CONTROL DAY 2

Fig. 5 Differences between the 48-hour forecast height fields over the region of interest, experimental minus control. Contour interval 0.5 dam.

over the region of interest, for the Eulerian scheme (Δt = 10 minutes) and Scheme B (Δt = 30 minutes). The dominant source of error in the Eulerian scheme appears to be the advection of spatial truncation error into the region of interest from the area of lower resolution outside. The effect is much less pronounced for Scheme B, which suggests that this scheme is giving significantly more accurate results over the non-uniform part of the grid. In the context of regional modelling, this result provides additional justification for the approach of using a non-uniform grid with the boundaries well away from the area of interest, since the semi-Lagrangian scheme handles more accurately the "driving flow" over the non-uniform part of the grid.

Thus, the study of Staniforth and Temperton (1986) demonstrated that a semi-implicit semi-Lagrangian scheme could be applied in a barotropic finite-element model. No problems were encountered with the non-uniform mesh. With a gridlength of 100 km over the region of interest, timesteps of up to 90 minutes (more than 6 times the stability limit of the Eulerian scheme) could be used with no significant loss of accuracy.

4. APPLICATION TO A SPECTRAL MODEL

In view of the similarities between the two methods of discretization, it was not altogether surprising that the semi-implicit semi-Lagrangian scheme, first developed for a gridpoint model, could be adapted for use in a finite-element model. It was perhaps less evident at the outset that such a scheme would also be applicable to spectral models.

In a first step towards this goal, Ritchie (1987) studied the semi-Lagrangian treatment of advection on the sphere, using a Gaussian grid. The test problem (advection of a passive scalar F by a steady wind field) may be written simply as

$$\frac{dF}{dt} \equiv \frac{\partial F}{\partial t} + \underset{\sim}{v}_H \cdot \nabla_H F = 0 \qquad (4.1)$$

where $\underset{\sim}{v}_H$ and ∇_H are the horizontal wind and gradient operator respectively.

In the context of a three-time-level scheme, a suitable semi-Lagrangian approximation to (4.1) would be

$$\frac{F^+ - F^-}{2\Delta t} = 0 \tag{4.2}$$

where F^+ is the value at a Gaussian gridpoint $\underset{\sim}{g}$ at time-level $(t+\Delta t)$, and F^- is the value at the upstream location $\underset{\sim}{r}^-$ at time-level $(t-\Delta t)$. In order to find the upstream location $\underset{\sim}{r}^-$, we first find the "halfway" point $\underset{\sim}{r}^0$ at time t. Spherical geometry introduces two complications: first, the natural analogue of (2.4) is

$$\underset{\sim}{r}^0(t) = \underset{\sim}{g} - \Delta t \dot{\underset{\sim}{r}}(t) \tag{4.3}$$

where $\dot{\underset{\sim}{r}}(t)$ is the velocity vector at $\underset{\sim}{r}^0(t)$. Since $\dot{\underset{\sim}{r}}(t)$ is tangent to the surface of the sphere, and $\underset{\sim}{g}$ is a Gaussian gridpoint on the sphere, (4.3) would lead to a position slightly off the sphere. To avoid this problem, a correction factor b is introduced to guarantee that $\left|\underset{\sim}{r}^0(t)\right| = a$, where a is the radius of the sphere:

$$\underset{\sim}{r}^0(t) = b\{\underset{\sim}{g} - \Delta t \dot{\underset{\sim}{r}}(t)\}. \tag{4.4}$$

It can be shown (Ritchie, 1987) that

$$b = \left[1 + (\Delta t)^2 \left|\dot{\underset{\sim}{r}}(t)\right|^2/a^2 - 2\Delta t \dot{\underset{\sim}{r}}(t) \cdot \underset{\sim}{g}/a^2\right]^{-\frac{1}{2}}$$

and that the factor b introduces an $O(\Delta t^2)$ correction. Hence the analogue of (2.5), to solve iteratively for the upstream point $\underset{\sim}{r}^0$, is

$$[\underset{\sim}{r}^0(t)]^{(k+1)} = b^{(k)} \{\underset{\sim}{g} - \Delta t[\dot{\underset{\sim}{r}}(t)]^{(k)}\}. \tag{4.5}$$

The second problem introduced by spherical geometry is that a straight line in (λ, θ) space is a poor approximation to a great circle trajectory, especially near the poles. The solution is to solve (4.5) in a three-dimensional Cartesian coordinate system (x,y,z) whose origin is at the centre of the sphere. The details of this algorithm are given by Ritchie (1987).

Once (4.5) has been solved for $\underset{\sim}{r}^0(t)$, the upstream point $\underset{\sim}{r}^-(t-\Delta t)$ is given by considering position vectors along a great circle trajectory:

$$\underset{\sim}{r}^-(t-\Delta t) = 2[\underset{\sim}{r}(t) \cdot \underset{\sim}{g}/a^2]\underset{\sim}{r}(t) - \underset{\sim}{g}. \tag{4.6}$$

Given the upstream point $\underset{\sim}{r}^{-}(t-\Delta t)$, the quantity F^{-} in (4.2) can be found by a suitable interpolation scheme (e.g., bicubic interpolation in (λ,θ) space).

As in the case of a polar stereographic projection (Section 2), a non-interpolating semi-Lagrangian approximation to (4.1) can also be developed (Ritchie, 1987). Here there is an additional impact of spherical geometry: even when the modified departure point $\underset{\sim}{r}^{*}(t-\Delta t)$ is chosen to be a point of the Gaussian grid, the half-way point $\underset{\sim}{r}^{*}(t)$ has no special relationship to the grid. Consequently, the full interpolation scheme is required to evaluate the residual advection.

Ritchie (1987) reported on a series of experiments in which a passive scalar with an initial "Gaussian hill" distribution was advected by a steady wind field corresponding to solid body rotation. The experiments were designed so that the "hill" passed directly over the pole after half a rotation. Eq. (4.1) was approximated by an Eulerian spectral scheme, and by both interpolating and non-interpolating semi-Lagrangian schemes. The results were compared against analytic solutions. It was shown that the semi-Lagrangian schemes could be stably and accurately applied to treat advection on the Gaussian grid with timesteps far exceeding the stability limit for the Eulerian spectral model. Both versions compared favourably with the Eulerian scheme in terms of accuracy, with some advantage for the non-interpolating scheme in the treatment of short scales.

The algorithms described above for the semi-Lagrangian treatment of advection on the sphere can now be coupled with the semi-implicit scheme in a barotropic spectral model (Ritchie, 1988). The shallow-water equations on the sphere may be written in the form

$$\frac{\partial U}{\partial t} + \frac{1}{a^2}\frac{\partial \overline{\phi}^{t}}{\partial \lambda} = -\{A(U,V,U) - fV\} \tag{4.7}$$

$$\frac{\partial V}{\partial t} + \frac{\cos\theta}{a^2}\frac{\partial \overline{\phi}^{t}}{\partial \theta} = -\{A(U,V,V) + fU + 2\sin\theta E\} \tag{4.8}$$

$$\frac{\partial \phi}{\partial t} + \Phi_0 \overline{D}^{t} = -\{A(U,V,\phi) + \phi D\} \tag{4.9}$$

where

$$U = \frac{u \cos\theta}{a}, \quad V = \frac{v \cos\theta}{a},$$

$$D = \frac{1}{\cos^2\theta}\left\{\frac{\partial U}{\partial \lambda} + \cos\theta \frac{\partial V}{\partial \theta}\right\},$$

$$E = \frac{1}{2}\left\{\frac{U^2 + V^2}{\cos^2\theta}\right\},$$

λ is longitude, θ is latitude, and $\overline{(\ )}^{t}$ indicates averaging in time for the semi-implicit scheme. The operator A is defined by

$$A(U,V,F) = \frac{1}{\cos^2\theta}\left\{U \frac{\partial F}{\partial \lambda} + V \cos\theta \frac{\partial F}{\partial \theta}\right\}$$

and represents the advection of F: thus

$$\frac{dF}{dt} \equiv \frac{\partial F}{\partial t} + A(U,V,F).$$

The basic barotropic spectral model was similar to that used by other researchers (e.g. Bourke, 1972), and immediately posed the same problem as that encountered for the finite-element model in Section 3: namely, the model was formulated in terms of the vorticity ζ and the divergence D. In preparation for the semi-Lagrangian treatment of advection, the model was first converted to U-V form, with the governing equations given by (4.7)-(4.9). It was shown (Ritchie, 1988) that this could be done without introducing an explicit spectral representation of U and V, and that the U-V and ζ-D versions of the model were algebraically equivalent.

A semi-Lagrangian treatment of the advection terms in (4.7)-(4.9) was then introduced, using the algorithms described earlier for the trajectory calculations in spherical geometry. Putting terms at time-levels t and $(t-\Delta t)$ on the right-hand side, the time-discretized form of the system (4.7)-(4.9) becomes:

$$\left(U + \frac{\Delta t}{a^2} \frac{\partial \phi}{\partial \lambda}\right)^{+} = Q_1 \qquad (4.10)$$

$$\left(V + \frac{\Delta t}{a^2} \cos\theta \frac{\partial \phi}{\partial \theta}\right)^{+} = Q_2 \qquad (4.11)$$

$$\left(\phi + \Delta t \Phi_0 D\right)^{+} = Q_3 \qquad (4.12)$$

As in the case of Cartesian coordinates, (4.10)-(4.12) lead to a Helmholtz

equation for ϕ^+:

$$\phi^+ - (\Delta t)^2 \Phi_0 \nabla^2 \phi^+ = Q_4 \qquad (4.13)$$

which is solved in the space of spherical harmonic coefficients.

However, an unexpected problem developed near the poles due to an instability associated with the metric term 2 sinθ E in (4.8) when a semi-Lagrangian treatment is used for the advection of V. A solution to this problem was found by considering the horizontal momentum equations (4.7)-(4.8) in vector form:

$$\frac{\partial \underset{\sim}{v}_H}{\partial t} + (\underset{\sim}{v}_H \cdot \nabla_H)\underset{\sim}{v}_H + f\underset{\sim}{k} \times \underset{\sim}{v}_H + \nabla_H \phi^t = 0 \qquad (4.14)$$

and integrating this equation in Cartesian coordinates on a local tangent plane at each gridpoint. A similar solution, for a semi-Lagrangian grid-point model on the sphere, has been put forward by Bates (1988). Again we obtain a system of the form (4.10)-(4.12), which is solved in the same way, but the definitions of Q_1 and Q_2 are altered. The trajectory calculations themselves are unchanged. The complete algorithm for both interpolating and non-interpolating semi-Lagrangian schemes is given by Ritchie (1988). [A slightly different solution to the problem of handling metric terms in the context of a semi-Lagrangian scheme has been proposed by Côté (1988).]

A set of model intercomparison experiments was then performed. The three U-V formulations (Eulerian, interpolating semi-Lagrangian and non-interpolating semi-Lagrangian) were run using a triangular T126 truncation. The timestep was Δt = 10 min for the Eulerian model, while the semi-Lagrangian models used a timestep of 1 hour. An integration of the Eulerian model with a T213 truncation (and Δt = 6 min) was used as a control run. The initial conditions were taken from a global 500 mb FGGE analysis, via nonlinear normal mode initialization.

The integrations were run out to 5 days; the forecast Northern Hemisphere height field for each model (T213 control and the three T126 models) is shown in Fig. 6. Notice the strong cross-polar flow, which apparently triggered the instability due to the metric term discussed earlier. Bearing in mind the length of the forecast, the differences are very small.

(a)

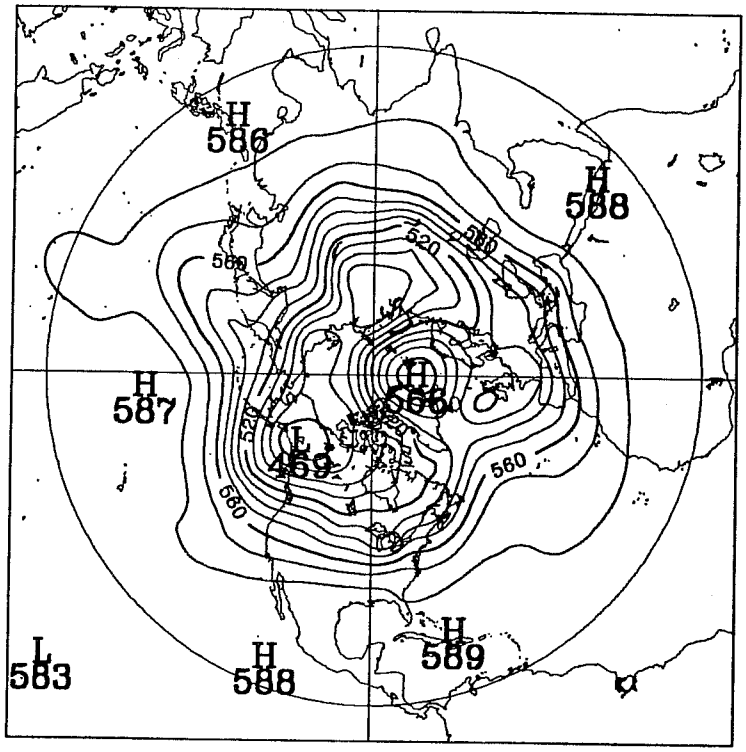

(b)

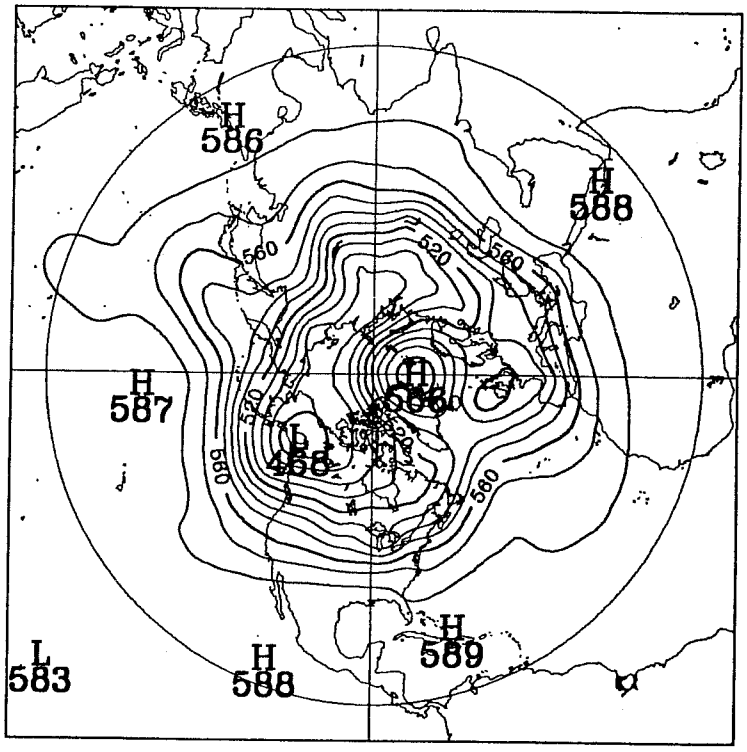

Fig. 6 5-day forecast height fields: (a) T213 control run, (b) T126 Eulerian model (Δt = 10 min). Contour interval 10 dam.

(c)

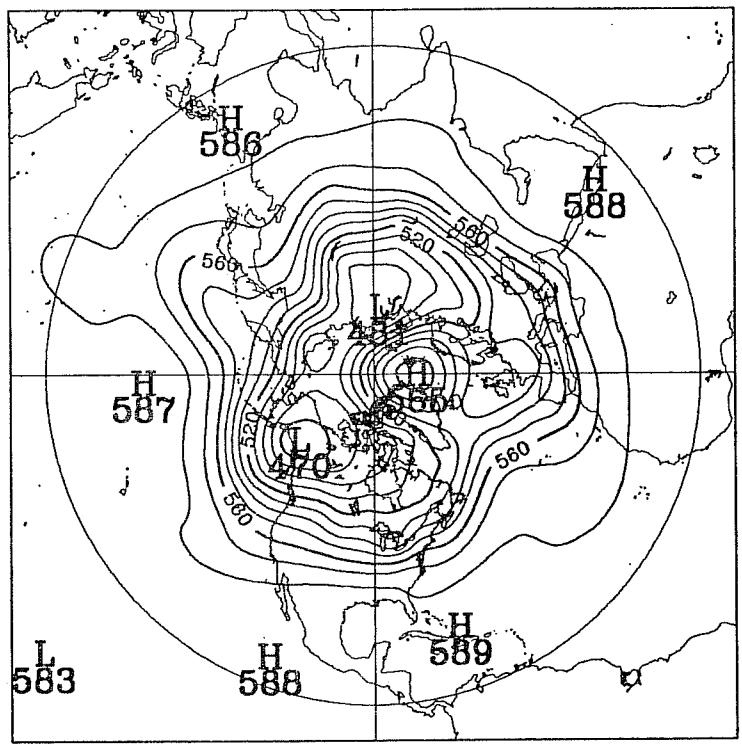

(d)

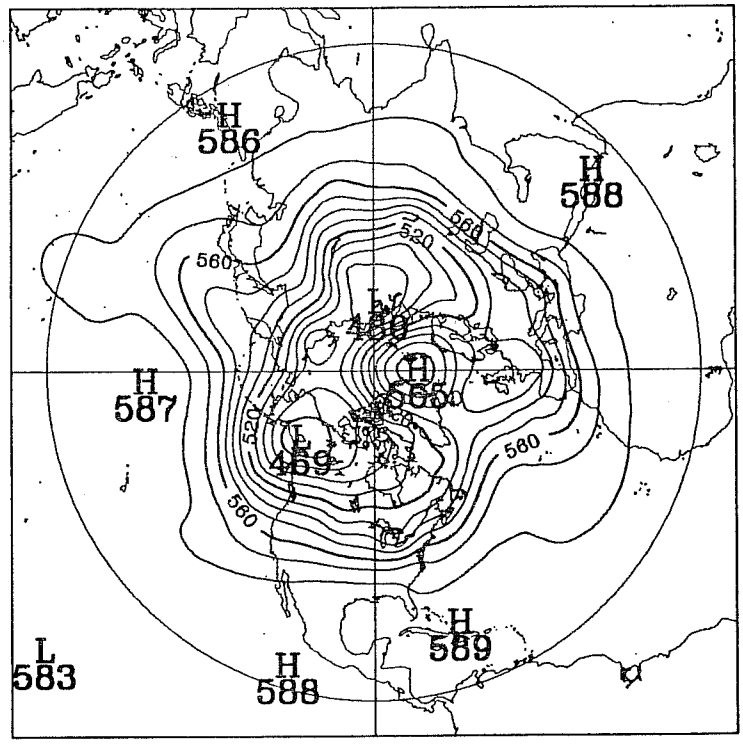

Fig. 6 (continued). 5-day forecast height fields: T126 semi-Lagrangian models, Δt = 60 min. (c) interpolating, (d) non-interpolating. Contour interval 10 dam.

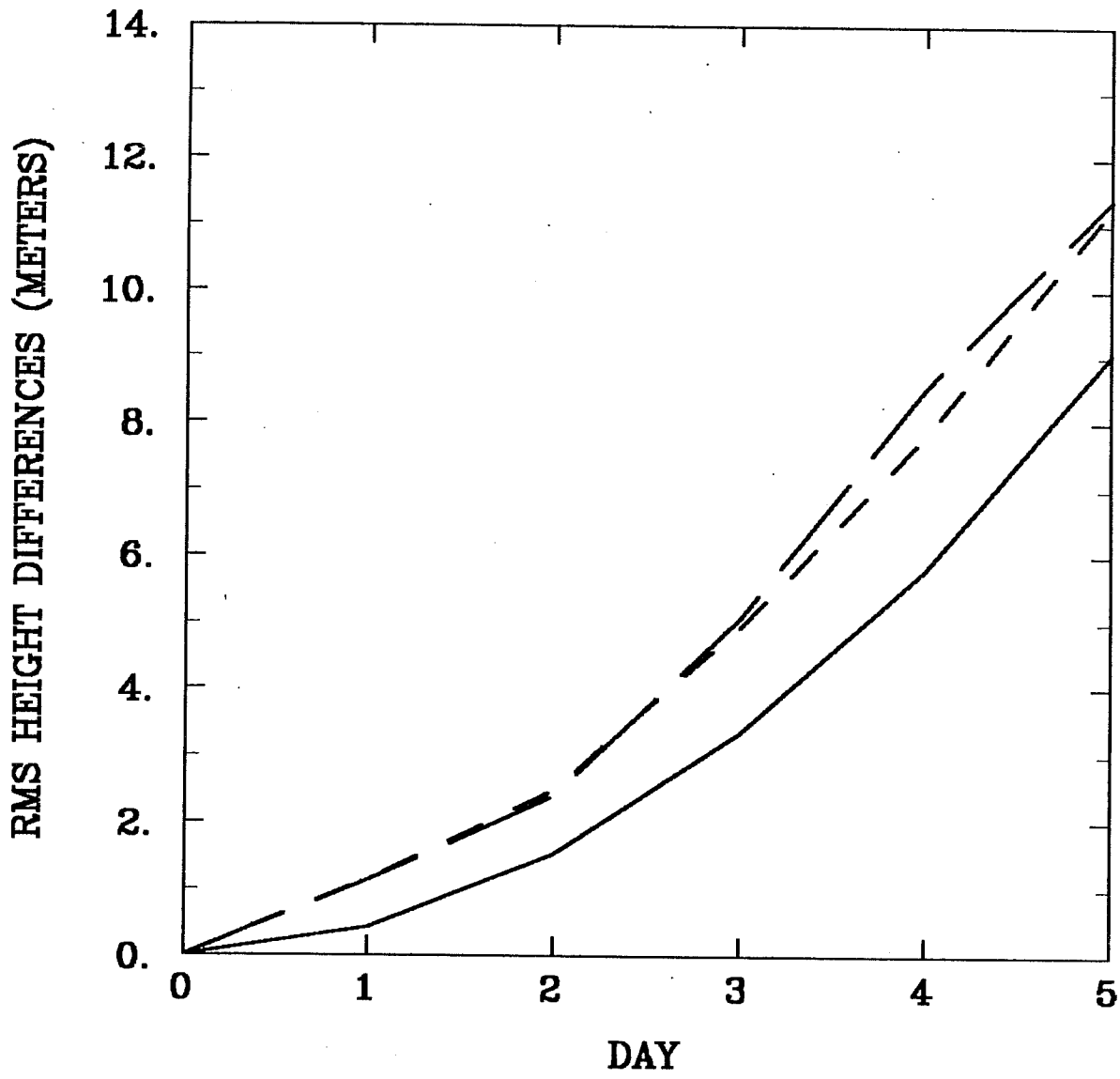

Fig. 7 Global rms height differences between experimental T126 and control T213 forecasts. Solid line, Eulerian model (Δt = 10 min). Long dashed line, interpolating semi-Lagrangian model (Δt = 60 min). Short dashed line, non-interpolating semi-Lagrangian model (Δt = 60 min).

For a more quantitative intercomparison, the global area-weighted r.m.s. differences between the forecast 500 mb height fields were calculated after each 24-hour interval. In Fig. 7 each T126 model is compared to the control run; the results show that the semi-Lagrangian models both give an accuracy which is quite acceptable in comparison with the Eulerian model at the same resolution.

Another point of some interest is the conservation of energy when the semi-Lagrangian schemes are used for long integrations. In order to examine this question, the two T126 semi-Lagrangian forecasts were extended to 20 days. The interpolating version was unfiltered, while the non-interpolating version included a time filter (Asselin, 1972) with a coefficient of 0.02. The evolution of potential (P), kinetic (K) and total (T) energy is presented in Fig. 8. The curves for the two models are almost indistinguishable, and the total energy is conserved to within about one per cent.

The study of Ritchie (1988) thus demonstrated that both interpolating and non-interpolating versions of the semi-implicit semi-Lagrangian scheme could be applied to a barotropic spectral model. At a resolution of T126, stable and accurate forecasts were run with a timestep of 1 hour, around 6 times the stability limit for an Eulerian model with the same resolution. It was also shown that the schemes could be used in 20-day integrations with negligible loss of energy.

5. CONCLUDING REMARKS

The studies of Staniforth and Temperton (1986) and Ritchie (1988) showed that three-time-level semi-implicit semi-Lagrangian schemes could be applied successfully to finite-element and spectral models of the shallow-water equations. Timesteps of the order of 60-90 minutes were used with acceptable accuracy, whereas the corresponding Eulerian models were restricted to timesteps of around 10 minutes because of the CFL stability criterion for the Eulerian treatment of advection. The stability criterion for the three-time-level semi-implicit semi-Lagrangian schemes is approximately $|f\Delta t| \leq 1$, and is a consequence of the explicit treatment of the

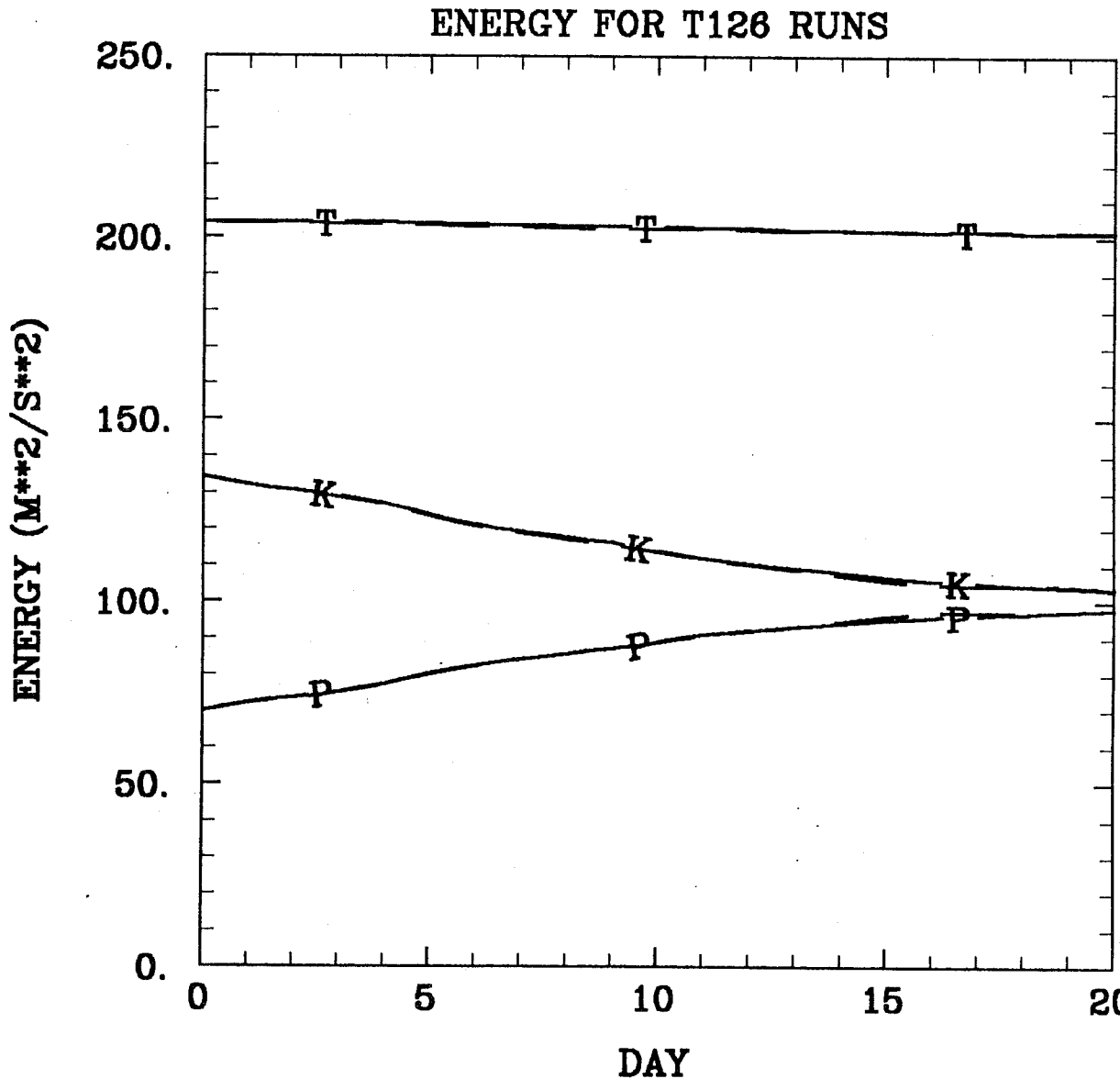

Fig. 8 Evolution of potential (P), kinetic (K) and total (T) energy during 20-day runs of the T126 semi-Lagrangian models. Solid line, non-interpolating model; dashed line, interpolating model.

Coriolis terms. With these schemes we are clearly in a better position to choose the timestep on the basis of accuracy rather than stability.

The real challenge now, of course, is to incorporate a semi-Lagrangian treatment of advection into the corresponding multi-level finite-element and spectral forecast models, as has already been done in a gridpoint model by Robert et al. (1985). At the time of writing (December 1987), the first successful experimental forecasts have already been run (Simard and Tanguay, personal communication) using a semi-Lagrangian version of the 15-level finite-element regional model of Staniforth and Daley (1979). In these forecasts, a fully three-dimensional semi-Lagrangian treatment of advection has been used. Meanwhile, work has started on coding a semi-Lagrangian version of the RPN spectral model (Béland and Beaudoin, 1985).

ACKNOWLEDGEMENTS

The authors wish to record their thanks to Maryse Ferland for her prompt and accurate typing of the manuscript.

REFERENCES

Asselin, R., 1972: Frequency filter for time integrations. Mon. Wea. Rev., 100, 487-490.

Bates, J.R., 1988: Finite-difference semi-Lagrangian techniques for integrating the shallow water equations on the sphere. ECMWF Workshop on Techniques for the Horizontal Discretization in NWP Models (this volume).

Béland, M. and C. Beaudoin, 1985: A global spectral model with a finite element formulation for the vertical discretization: adiabatic formulation. Mon. Wea. Rev., 113, 1910-1919.

Bourke, W., 1972: An efficient, one-level, primitive equation spectral model. Mon. Wea. Rev., 100, 683-689.

Côté, J., 1988: A Lagrange multiplier approach for the metric terms of semi-Lagrangian models on the sphere. Submitted to Quart. J. Roy. Met. Soc.

Kwizak, M. and A.J. Robert, 1971: A semi-implicit scheme for grid point atmospheric models of the primitive equations. Mon. Wea. Rev., 99, 32-36.

Ritchie, H., 1986: Eliminating the interpolation associated with the semi-Lagrangian scheme. Mon. Wea. Rev., 114, 135-146.

Ritchie, H., 1987: Semi-Lagrangian advection on a Gaussian grid. Mon. Wea. Rev., 115, 608-619.

Ritchie, H., 1988: Application of the semi-Lagrangian method to a spectral model of the shallow water equations. Mon. Wea. Rev., 116 (to appear).

Robert, A.J., 1969: The integration of a spectral model of the atmosphere by the implicit method. Proc. WMO/IUGG Symposium on Numerical Weather Prediction, Tokyo, Section VII, 19-24.

Robert, A.J., J. Henderson and C. Turnbull, 1972: An implicit time integration scheme for baroclinic models of the atmosphere. Mon. Wea. Rev., 100, 319-335.

Robert, A.J., 1981: A stable numerical integration scheme for the primitive meteorological equations. Atmos.-Ocean, 19, 35-46.

Robert A.J., 1982: A semi-Lagrangian and semi-implicit numerical integration scheme for the primitive meteorological equations. J. Met. Soc. Japan, 60, 319-325.

Robert, A.J., T.L. Yee and H. Ritchie, 1985: A semi-Lagrangian and semi-implicit numerical integration scheme for multilevel atmospheric models. Mon. Wea. Rev., 113, 388-394.

Staniforth, A.N. and H.L. Mitchell, 1977: A semi-implicit finite-element barotropic model. Mon. Wea. Rev., 105, 154-169.

Staniforth, A.N. and H.L. Mitchell, 1978: A variable-resolution finite-element technique for regional forecasting with the primitive equations. Mon. Wea. Rev., 106, 439-447.

Staniforth, A.N. and R.W. Daley, 1979: A baroclinic finite element model for regional forecasting with the primitive equations. Mon. Wea. Rev., 107, 107-121.

Staniforth, A. and C. Temperton, 1986: Semi-implicit semi-Lagrangian integration schemes for a barotropic finite-element regional model. Mon. Wea. Rev., 114, 2078-2090.

Staniforth, A. and J. Côté, 1988: Two-time-level semi-Lagrangian schemes in finite-element and spectral models. ECMWF Workshop on Techniques for Horizontal Discretization in NWP Models (this volume).